

# Impact of Wall Temperature on Aerothermal Characteristics of an Array of Surface Microstructures

**D. Campanaro**

Department of Engineering Science  
University of Oxford  
Oxford OX2 0ES, UK  
Email: domenico.campanaro@eng.ox.ac.uk

**L. He**

Department of Engineering Science  
University of Oxford  
Oxford OX2 0ES, UK  
Email: li.he@eng.ox.ac.uk

## ABSTRACT

*The aero-thermal behavior of surface microstructures is of wide relevance, especially given the development of additive manufacturing (AM). Of particular interest is the interaction between fluid flow and heat transfer. In the present work, two contrasting configurations, a flat plate boundary layer and an array of hemispheric microstructures are examined at three wall-inflow temperature ratios (TR): cooled (TR=0.5), adiabatic (TR=1) and heated wall (TR=1.5). Due to a compensation between fluid viscosity and velocity gradient in the boundary layer, the heat transfer effects may appear deceptively small if judged using the common aerothermal parameters ( $C_f, Nu$ ). The authors find instead the local Reynolds number to be more usefully indicative of such aerothermal interaction. The scale-resolving LES simulations at a range of Reynolds numbers show that the cooled wall case is characterized by a markedly earlier transition which takes place at a much lower (by 50%) bulk flow Reynolds number compared to a near-adiabatic case. Furthermore, it is shown that the incompressible flow LES solutions fail to capture the early transition under the same cooling condition. Finally, a regrouping of the non-dimensional parameters ( $C_D, Nu$ ) with TR is proposed leading to a more unified characterization for easier scaling of wall heat transfer effects in practical applications.*

## Nomenclature

$\eta$  Blasius non-dimensional y-coord.; ( $y\sqrt{u_\infty\rho_\infty/\mu_\infty x}$ )  
 $\rho$  density  
 $\mu$  dynamic viscosity  
 $\tau_w$  wall shear stress  
 $C_D$  drag coefficient; ( $C_{D_f} + C_{D_p}$ )  
 $C_{D_f}$  frictional drag coefficient  
 $C_{D_p}$  pressure drag coefficient  
 $C_f$  local frictional drag coefficient  
 $D_{tot}$  local Reynolds number difference  
 $h$  or  $HTC$  heat transfer coefficient; ( $q/(T_w - T_{01})$ )  
 $I$  turbulence intensity  
 $k$  free-stream thermal conductivity  
 $L$  flat plate length  
 $Nu_L$  flat plate Nusselt number based on  $L$   
 $Nu_r$  surface microstructure Nusselt number based on  $r$

$Nu_{ref}$  reference Nusselt number  
 $Pr$  Prandtl number  
 $q$  heat flux  
 $r$  pin radius  
 $Re_{local}$  local Reynolds number  
 $Re_L$  Reynolds number based on  $L$ ;  $(\rho_{\infty} u_{\infty} L / \mu_{\infty})$   
 $Re_r$  Reynolds number based on  $r$ ;  $(\rho_{\infty} u_{\infty} r / \mu_{\infty})$   
 $\Delta t_{nd}$  non-dimensional time step; *(time step/throughflow time)*  
 $T_{01}$  inlet total temperature  
 $T_w$  wall temperature  
 $TR = T_w / T_{01}$  temperature ratio  
 $u$  velocity

## 1 Introduction

In recent years, the development of Additive Manufacturing (AM)/‘3D printing’ technology has generated significant academic and industrial interest due to its capability to produce complex geometries at an affordable cost. Additive manufacturing can be used, for instance, to form specific surface finish patterns/‘regular roughness’. Arrays of spatially distanced surface microstructures can be printed on a surface and potentially lead to a performance gain for many devices and machines in power generation and aviation industries.

It is well known that surface finish in general can have a substantial impact on the aerothermal characteristics of the flow bounded by the surface [1–8]. Given the huge amount of previous research efforts made on the conventional stochastic surface roughness, it should be useful to consider if we can learn from the understanding and characterization of random roughness, which might apply to the manufacturable regular roughness. Parameters such as sand-grain height  $k_s$ , centerline height  $R_a$ , mean height  $\mu$ , roughness skewness, and peak-to-valley distance, are currently used to characterize conventional roughness. Nevertheless, various previous researches indicate that those criteria are inadequate, and that the detailed roughness topography should be taken into account as well [9–15]. Even for those well-established parameters, their restricted applicability can also be exposed for regular roughness. An example is the ‘roughness slope’ (the roughness element size normalized by the element-to-element length scale/wavelength  $R_a/\lambda$ ) for an improved characterization for random roughness topology, Goodhand et al [16]. On the other hand, an examination on regular roughness by Kapsis and He [17] shows a strong directionality of the impact of the element-to-element length-scale, which thus illustrates the inadequacy of a single roughness spacing parameter such as  $R_a/\lambda$ . The corresponding results for regular micro-structures underline that the detailed shapes and patterns of regular roughness have considerable effects on aerodynamic and heat transfer performance of practical interest.

Various studies have been conducted to assess the impact of additively manufactured microstructures in different engineering applications such as turbomachinery [18–20], and micro-electro-mechanical systems [21]. Ferster et al [20], for instance, adopted direct metal laser sintering (DMLS) to manufacture pin-fin arrays for turbine blade internal cooling, where the effect of micro-structure geometries (triangular, star, and dimpled spherical shapes), and spacing patterns on aerodynamics (pressure losses) and heat transfer were tested and analyzed. The work of Miao et al [22] shows that engineered surface structures might be used to control the secondary flow in a turbine blade passage and reduce its intensity to improve cooling effectiveness.

The sensitivities of the aerothermal performance to detailed shapes and patterns of regular roughness provide a motivation to develop computational methods to be able to resolve, rather than empirically model, the flow around these microstructures. The major challenge faced then is to solve the flow field around a huge number of microstructures to predict the effect on a typical micro-structured surface of interest. This is a typical two-scale problem since the high gradient flow around each element requires a fine local mesh, making it prohibitive to solve if a direct single-scale solution strategy is simply adopted. In the past, various multi-scale techniques have been developed to deal with different spatial and temporal scales in general [23, 24]. Recently, He [25] has developed a two-scale block-spectral approach for unsteady flows capable of resolving the flow field around surface microstructures at an affordable cost. The development of multi-scale methods presents considerable potential for applications to AM manufacturable surface micro-structures as indicated by Kapsis et al [26].

When examining a flow field around surface microstructures, we should also consider the relation and potential interplay between two basic aspects of interest: aerodynamics and convective heat transfer. Conventional wisdom tends to regard the convective heat transfer to be completely determined by aerodynamics. In terms of the Newton’s law of cooling, the heat transfer coefficient (HTC) is taken to be independent of the wall temperature, equivalently the flow field is unaffected by wall heat transfer. Such conventional wisdom has been often questioned (e.g. Moffat [27]). There are some empirical correlations developed to account for temperature ratio (TR) effects, but they are largely based on turbulent flat plate boundary layer flows [28, 29]. More recently, the inter-dependence between aerodynamics and heat transfer has been studied for more

realistic high pressure turbine blade geometry, by Maffulli and He [30,31] and by Zhang and He [32]. Their work shows that neglecting the influence of wall temperature on the HTC might lead to inaccurate heat transfer predictions by more than 20% for transonic turbine blades. Additionally, the analysis by Maffulli and He [31] indicates that wall cooling may promote an earlier boundary layer transition on the blade surfaces. This observation should be taken with caution however as the results were obtained from RANS calculations.

For the laminar-turbulent transition, the impact of wall cooling/heating has been studied by various previous research efforts. In the supersonic flow regime, Shadloo [33], for instance, studied the influence of heat transfer on transition in supersonic boundary layers. Their DNS results show an earlier transition in the case of wall cooling in contrast to the linear stability theory that predicts the opposite. Other researchers focused on supersonic flows over cone nose-tip geometries [34–37]. Buntin et al [35], for instance, show that for sharp nose-tips cooling and heating would have correspondingly a stabilizing and destabilizing effect respectively. On the other hand, Buntin et al [35] also report the opposite behavior for blunt nose-tips: cooling and heating would promote and delay transition respectively.

In the subsonic flow regime, Schafer and Ozgen [38,39] modified the incompressible stability equations to account for the variation of temperature dependent fluid properties across the boundary layer and found that cooling would destabilize low speed water flows but stabilizes air flows. Their results are compared with the experimental work by Liepmann and Fila [40] who also highlighted the stabilizing effect of cooling on air flows. In contrast with the aforementioned findings referred to a natural transition, other studies [41–43] show that cooling promotes the bypass transition even if such behavior is opposite to what was expected from the small disturbance stability theory. These results nevertheless seem to be qualitatively in agreement with those observed experimentally by Back et al [44]. Overall observations regarding the impact of wall heat transfer on the laminar-turbulent flow transition still seem to be inconclusive. Furthermore, we note that those aforementioned previous research efforts on transition are all for smooth surfaces. Very little has been done in analyzing the transition under influence of wall heat transfer for surface microstructures.

Given the state of the art as reviewed above, the present work is aimed to address the relation and possible interplay between aerodynamics and convective heat transfer for surface microstructures, and particular attention is paid to the transitional flow regime. We ask several specific questions for the flow around surface microstructures under wall cooling/heating:

- How would the variations in the local flow field and local fluid properties caused by heat transfer affect aerothermal performance?
- How would the local flow and fluid property changes influence the Reynolds number, and how should we evaluate those effects?
- How would an incompressible flow model behave in predicting transition under the influence of heat transfer (particularly given the incompressible model being often adopted for transition studies)?

The rest of the paper is organized as follows. In section 2, the computational method and case set-ups are introduced. In section 3, the laminar boundary layer on a flat plate is first presented for a validation. The results at different wall temperatures are then compared to highlight how the wall heat transfer may influence the flow field, fluid properties, and performance parameters in rather different while consequential ways. In section 4, the flow field around an array of micro-structures are analyzed for a fully laminar and a fully turbulent flow respectively. Emphasis is on how the changes of local flow velocity, and fluid properties due to heat transfer can alter most relevantly the local Reynolds number. Additionally, the transition behavior under different nominal Reynolds numbers is computed at different TRs. The results are also contrasted with those predicted by an incompressible flow model to address its applicability under the influence of heat transfer, even though in a nominally incompressible low-speed flow regime. The calculated aerothermal performance results in the transition regime are also further reformulated to account for the temperature ratio in a unified non-dimensional form independent of the amount of wall heat transfer. Finally some concluding remarks are presented.

## 2 Computational method and set-up

Large eddy simulations (LES) are performed to solve the compressible Navier-Stokes equations. Low speed flows have been analysed ( $M < 0.3$ ), and the compressible flow model is used to capture the effects on the flow field of fluid properties variations due to heat transfer. The commercial codes ANSYS ICEM and FLUENT are used for mesh generation and flow simulation, respectively. A pressure-based finite volume method with a pressure-velocity coupled scheme is adopted.

The inlet total temperature  $T_{01}$  is taken to be 280K, and the wall temperature is set to a uniform value to match the prescribed temperature ratio (TR), defined as  $T_w/T_{01}$ . Air properties such as thermal conductivity and specific heat capacity vary with temperature according to air properties tables. Dynamic viscosity is based on Sutherland's law and density on the ideal gas law. The exit pressure is set to atmospheric pressure. Performance parameters are calculated as follows:

- Nusselt number:  $Nu_L = \frac{hL}{k}$ , or  $Nu_r = \frac{hr}{k}$
- Drag coefficient:  $C_D = C_{D_f} + C_{D_p}$

Two different set-ups are used in the present study and described in the following sub-sections: flat plate boundary layer, and surface microstructure array.

## 2.1 Flat plate boundary layer

The flow domain is illustrated in fig. 1. The upstream part of the domain is inviscid, so the boundary layer starts at the leading edge location indicated in fig. 1, where the viscous wall begins. The top boundary is specified to be an inviscid wall.

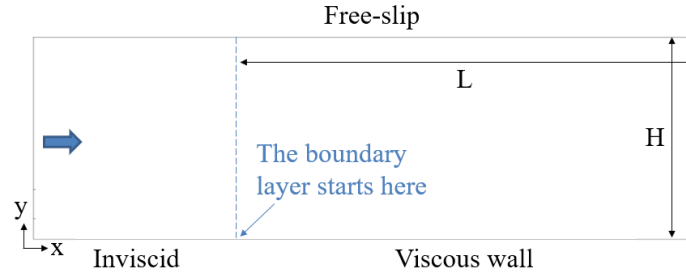


Fig. 1: Flat plate boundary layer domain (height and length are to the scale  $H/L=2.5$ ).

## 2.2 Surface microstructure array

In this case, the bottom surface of the domain is subject to a row of eight hemispherical micro-structures of radius  $r$  in the streamwise direction with periodic side boundaries in the  $z$ -direction, as illustrated in fig. 2. No-slip and free-slip conditions are applied respectively to the wall surface and the top boundary. The inlet total pressure profile is prescribed so that the resulting inlet velocity profile is always laminar and matches the Blasius solution. The inlet boundary layer thickness is fixed to  $20r$ . Various Reynolds number values ( $Re_r$ ) are tested by adjusting the total pressure profile.

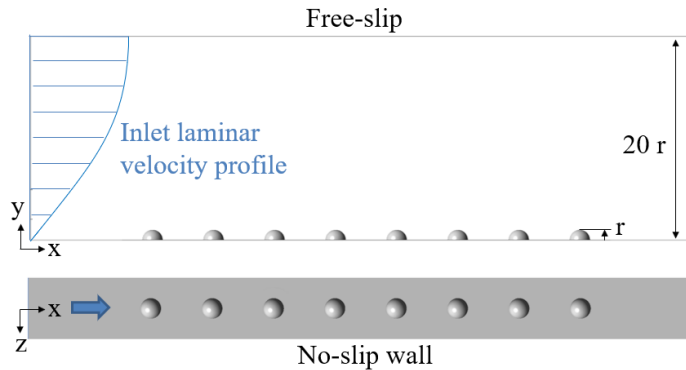


Fig. 2: Surface microstructure array domain: a row of eight hemispherical surface microstructures of  $500\mu\text{m}$  radius

## 3 Flat plate boundary layer

This section serves as a basic validation, and assesses the influence of fluid property and velocity variations, due to wall heat transfer, on performance parameters. Additionally, a local Reynolds number parameter is introduced to describe the impact of wall cooling/heating on the flow field. The flow domain used is described in section 2.1.

### 3.1 Basic validation and mesh sensitivity

A 2D mesh is produced using ANSYS ICEM, and a mesh refinement study is carried out testing three different mesh sizes in adiabatic conditions at  $Re_L=130000$ . All grids produce consistent results in agreement with the Blasius solution, as illustrated in fig. 3. The mesh used for this effectively 2D case is composed of 300k elements.

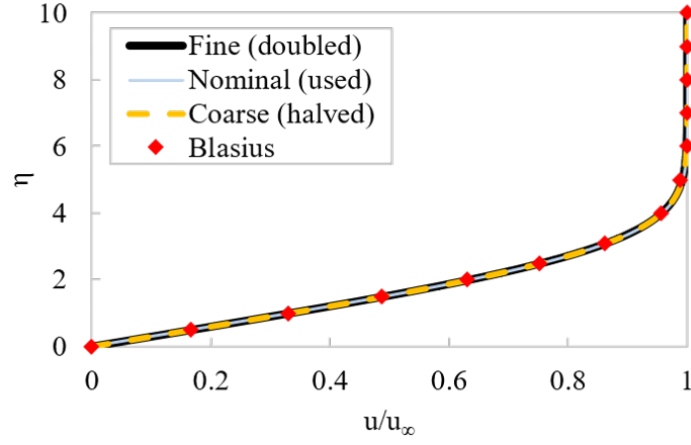


Fig. 3: Mesh dependency study for flat plate boundary layer

### 3.2 Impact of wall temperature

Three different wall temperatures are tested keeping the same Reynolds number value  $Re_L=130000$ :  $TR=0.5$  (cooled wall),  $TR=1$  (adiabatic), and  $TR=1.5$  (heated wall). Different TRs necessarily lead to different temperature fields, thus rather than looking at changes in the temperature field with TRs, a more relevant aspect is how the flow (velocity) field may respond to the wall heat transfer. The resulting velocity profiles are compared with the Blasius solution. Wall heating significantly thickens the boundary layer, in agreement with what was reported by Arnal [42], and the opposite trend is detected for wall cooling, as illustrated in fig. 4.  $TR=1.5$  and  $TR=0.5$  show respectively a  $\pm 20\%$  variation in boundary layer thickness.

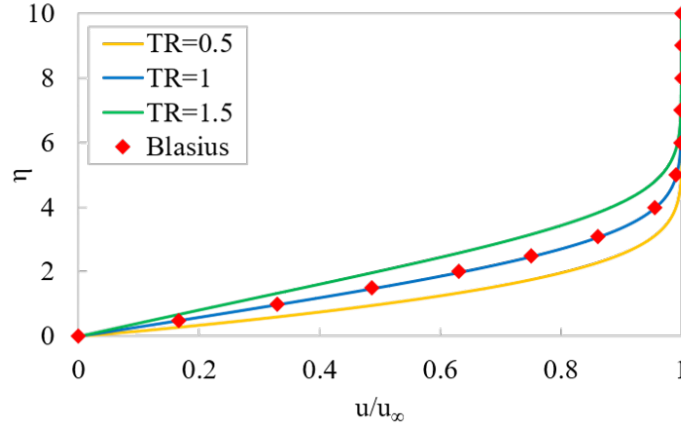


Fig. 4: Impact of TR on the velocity profile

To measure the influence of wall cooling/heating on performance parameters,  $TR=1.5$  and  $TR=0.5$  are compared with the adiabatic case ( $TR=1$ ). The Nusselt number for  $TR=1$  is obtained using the Reynolds-Colburn analogy as shown in eq. (1). The reason for the Nusselt number at  $TR=1$  not being taken from the simulation is that  $Nu$  is effectively a non-dimensional heat flux  $q$ , normalized by the driving temperature difference ( $T_{01}-T_w$ ) and other parameters. For the adiabatic case ( $TR=1$ ), the normalization of  $q$  will singularly fail (i.e.  $T_{01}-T_w=0$ ). Therefore, the Reynolds-Colburn analogy (where  $q$  is not explicitly needed) is used instead.

$$Nu_{L_{TR1}} = \frac{C_{D_{f_{TR1}}}}{2} Re_L Pr^{1/3} \quad (1)$$

In a seemingly contradictory behavior with the significant effect on the velocity profile depicted in fig. 4, the impact of TR on the drag coefficient and Nusselt number appears to be quite small, as reported in table 1.

Table 1: Impact of TR on performance parameters

$TR$	$Nu_L / Nu_{L_{TR1}}$	$C_{D_f} / C_{D_{f_{TR1}}}$
0.5	1.01	1.03
1.5	0.98	0.97

The explanation for this rather contradicting observation is the compensating effect of viscosity and velocity gradient on wall shear stress ( $\tau_w = \mu \frac{\partial u}{\partial y}$ ). Wall cooling, for instance, causes viscosity to drop significantly in the near-wall region. On the other hand, the velocity gradient substantially increases due to the velocity profile variation, as illustrated in fig. 5. The adiabatic values of viscosity and velocity gradient at the wall are used as reference in fig. 5.

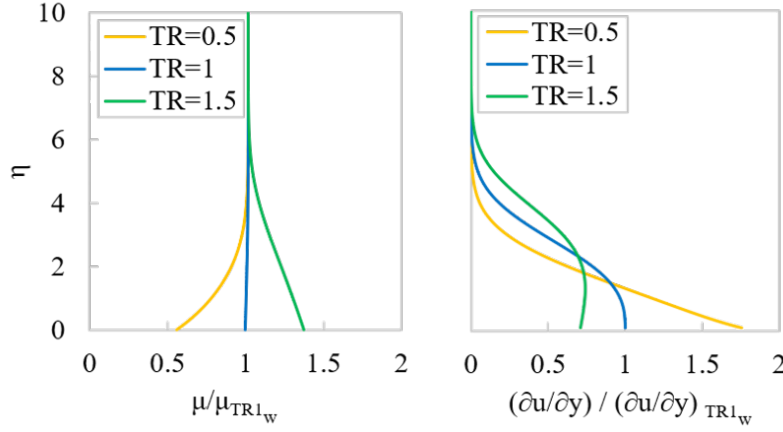


Fig. 5: Profiles of dynamic viscosity and velocity gradient at different wall temperature conditions non-dimensionalized using adiabatic values at the wall

The effects of TR on viscosity and velocity gradient cancel each other out leading to  $C_{D_f} / C_{D_{f_{TR1}}} \sim 1$ . Similarly, in the case of wall heating ( $TR=1.5$ ), viscosity goes up and velocity gradient decreases in the proximity of the wall, implying an exiguous variation of the frictional drag coefficient. The compensating effects of viscosity and velocity gradient result in a negligible net impact of TR on performance parameters, which effectively masks the substantial differences in the flow field caused by wall cooling/heating. A question then arises: which parameter is more suitable to describe the impact of TR on flat plate boundary layer flows? The definition of Reynolds number based on free-stream variables overlooks the significant variation of fluid properties and velocity profile in the boundary layer caused by heat transfer. To assess the influence of the wall heat transfer on the flow field across a boundary layer, Maffulli and He [30] introduced a nondimensional aerothermal parameter that represents the local Reynolds number, and is calculated using local fluid properties and velocity. Similarly, in the present study, a local Reynolds number is defined as a function of  $x$  and  $\eta$  in eq. (2), which should not be mistaken with the commonly used Reynolds number based on local distance  $Re_x = \rho_\infty u_\infty x / \mu_\infty$ .

$$Re_{local}(x, \eta) = \frac{\rho(x, \eta) u(x, \eta) x}{\mu(x, \eta)} \quad (2)$$

At any given  $x$  location, the  $Re_{local}$  profile is a function of the wall normal distance  $\eta$  only. The impact of TR on  $Re_{local}(\eta)$  is quantified in fig. 6, where the local Reynolds number profiles are depicted for three different wall temperatures. Wall cooling implies higher near-wall density, lower viscosity, and a thinner boundary layer (BL). All those effects contribute to increasing the local Reynolds number as illustrated in fig. 6.

Now we consider the cooled wall case more closely. Differently from the performance parameters for which viscosity and velocity gradient play a compensating role, fluid properties and velocity variations caused by wall cooling have an additive effect on the local Reynolds number. Therefore, to separately assess the contributions of velocity, density and viscosity, additional parameters are defined in eq. (3):  $D_{tot}(\eta)$  is the total variation in the local Reynolds number;  $D_u(\eta)$

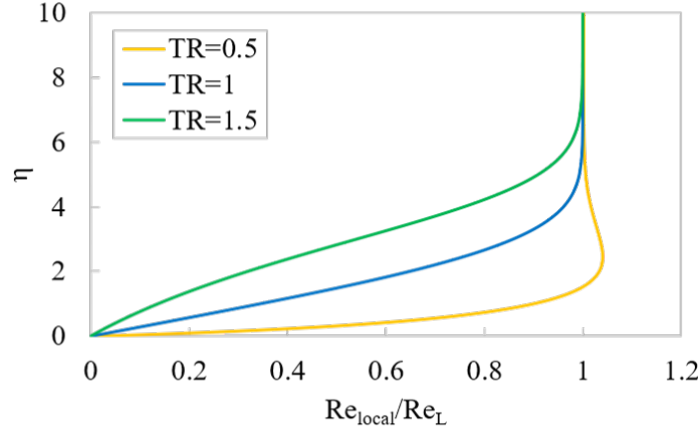


Fig. 6: Local Reynolds number profile

measures the influence of velocity variations due to wall cooling on the local Reynolds number profile;  $D_\rho(\eta)$  the influence of density; and  $D_\mu(\eta)$  the influence of viscosity. The value of the local Reynolds number at the adiabatic condition ( $TR=1$ ) is taken as the reference.

$$\begin{aligned}
 Re_{local}(\eta)_{TR1} &= \frac{\rho(\eta)_{TR1} u(\eta)_{TR1} x}{\mu(\eta)_{TR1}} \\
 D_{tot}(\eta) &= \frac{Re_{local}(\eta)_{TR05} - Re_{local}(\eta)_{TR1}}{Re_{local}(\eta)_{TR1}} \\
 D_u(\eta) &= \frac{\frac{\rho(\eta)_{TR1} u(\eta)_{TR05} x}{\mu(\eta)_{TR1}} - Re_{local}(\eta)_{TR1}}{Re_{local}(\eta)_{TR1}} \\
 D_\rho(\eta) &= \frac{\frac{\rho(\eta)_{TR05} u(\eta)_{TR1} x}{\mu(\eta)_{TR1}} - Re_{local}(\eta)_{TR1}}{Re_{local}(\eta)_{TR1}} \\
 D_\mu(\eta) &= \frac{\frac{\rho(\eta)_{TR1} u(\eta)_{TR1} x}{\mu(\eta)_{TR05}} - Re_{local}(\eta)_{TR1}}{Re_{local}(\eta)_{TR1}}
 \end{aligned} \tag{3}$$

The contributions of velocity, density and viscosity variations, due to wall cooling, on the local Reynolds number profile, are represented in fig. 7. Those results lead to the following observations: the three parameters  $D_u$ ,  $D_\rho$ , and  $D_\mu$ , show a significant impact near the wall (roughly about 90% each); the contribution of density is the most significant at the wall; for  $\eta > 0.5$ , velocity is the most impactful factor in increasing the local Reynolds number; the contribution of density is larger than that of viscosity.

In the proximity of the wall ( $\eta < 1$ ), for  $TR=0.5$ ,  $Re_{local}(\eta)$  reaches values five times higher than the adiabatic profile ( $TR=1$ ). The near-wall effect is considerable in the case of wall heating ( $TR=1.5$ ) as well,  $Re_{local}(\eta)$  is reduced by over 60% (see fig. 6). The significant impact of TR on the local Reynolds number distribution is not confined to the near-wall region, and affects almost an entire boundary layer up to  $\eta=5$ .

These  $Re_{local}$  profiles clearly illustrate that heat transfer has a non-negligible impact on the flow field even if frictional drag coefficient and Nusselt number do not reflect such an effect. Thus, one can be easily misguided if judging the influence of wall heat transfer on aerodynamic flow field merely based on these two basic aerothermal performance parameters.

In the next section, the local Reynolds number variation due to wall cooling/heating, as well as its implication on aerodynamics, will be studied for a surface microstructure array.

#### 4 Surface microstructure array

In this section, the interdependence between heat transfer and aerodynamics is analysed for a surface microstructure array at different Reynolds numbers ranging from laminar to turbulent flows. The flow domain is shown in fig. 2 as described in section 2.2. The inlet total pressure profile is specified so that the resulting inlet velocity profile is laminar and matches the Blasius solution as illustrated in fig. 8.

For low  $Re_\tau$  (laminar cases), the flow over the microstructures leads to a steady recirculation region (fig. 9a). On the other hand, for higher Reynolds numbers (turbulent cases), turbulent separation takes place (fig. 9b), and a scale-resolving

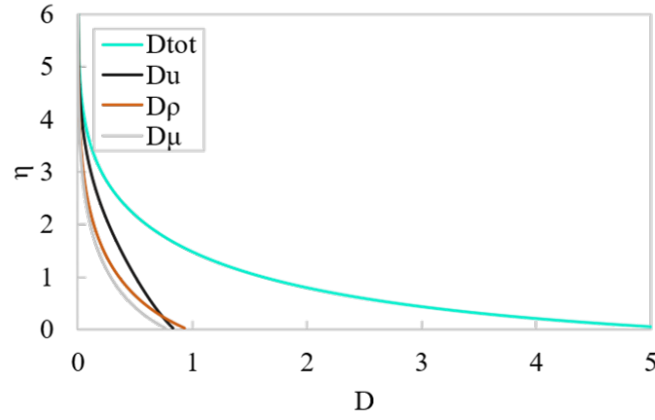


Fig. 7: The contribution of velocity, dynamic viscosity, and density to increasing  $Re_{local}$  in the near-wall region for  $TR=0.5$

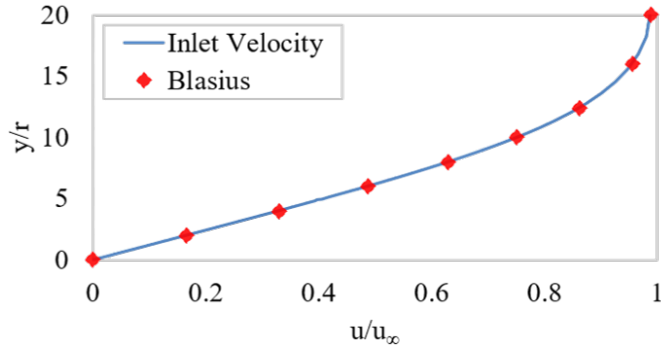


Fig. 8: Inlet velocity profile, obtained by specifying a total pressure profile to match the laminar Blasius solution as shown

approach is required. The LES method is adopted without an explicit sub-grid model. This is effectively an implicit LES, and is preferred to capture a transition process without the subgrid model interfering with the laminar flow part, e.g He [45].

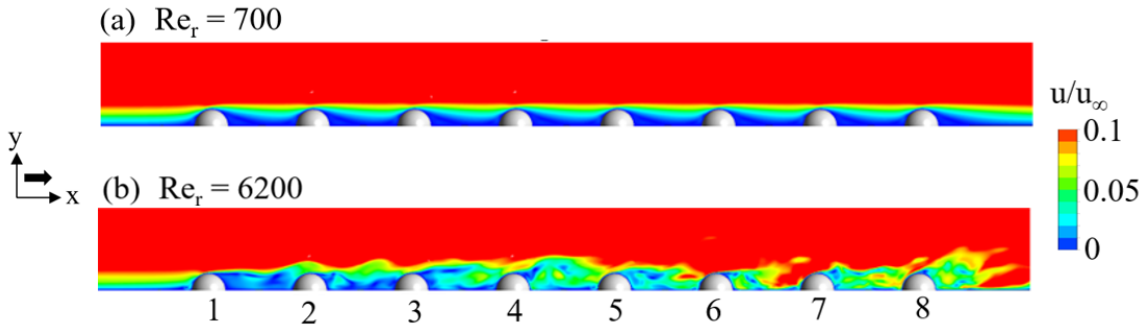


Fig. 9: Velocity contours, a) Laminar flow field  $Re_r=700$ , b) Turbulent flow field  $Re_r=6200$

Vorticity iso-surfaces for a laminar and a turbulent case are presented in fig. 10. To achieve consistent laminar and LES results, mesh and time step sensitivity studies are carried out as described in the next section.

#### 4.1 Numerical sensitivity study

The assessment of numerical sensitivity is carried out for a surface microstructure array in the turbulent regime ( $Re_r=4000$ ) with  $TR=0.5$ . A 3D mesh is generated using ANSYS ICEM. A structured multiblock approach is adopted to consistently refine the near wall region. The flow domain around each hemispheric microstructure is meshed with an o-grid as depicted in fig. 11.



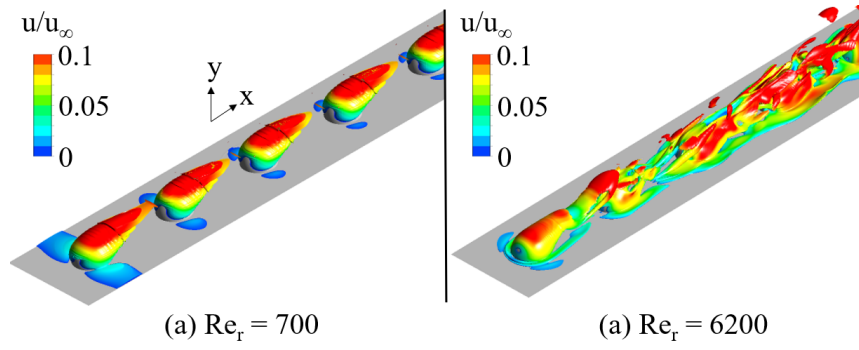


Fig. 10: Vorticity iso-surfaces colored with  $u$  values: a) laminar, b) turbulent

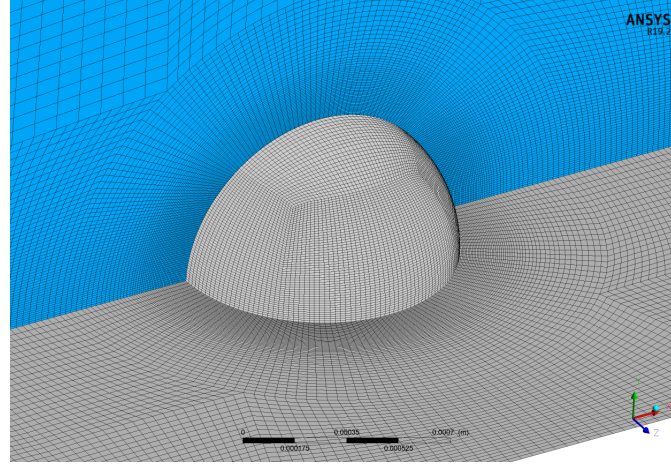


Fig. 11: O-grid mesh around one of the microstructures

For the mesh dependency study, two grids are tested: 10M and 15M elements. The discrepancy caused by using the coarse mesh (10M) is less than 1% as reported in table 2. Similarly, in the time step dependency study, two time step sizes are assessed:  $\Delta t_{nd}=0.002$ , and  $\Delta t_{nd}=0.001$ , see table 3. Given the small discrepancies, a 10M element mesh, and a time-step size of  $\Delta t_{nd}=0.002$  are considered sufficiently accurate to resolve turbulent cases.

Table 2: Mesh size sensitivity

$Mesh\ size$	$\overline{Nu_r}$
10M	5.30
15M	5.29

Table 3: Time step size sensitivity

$\Delta t_{nd}$	$\overline{Nu_r}$
0.002	5.30
0.001	5.32

For laminar cases, convergence is assumed when a steady state is reached. For turbulent cases, convergence is measured based on time-averaged Nusselt number. It is observed that after a sampling period of 5 through-flow times, the differences between two through-flow periods fall to less than 2%, as illustrated in fig. 12. Sampling starts once the flow field is judged to be fully developed, which is reached after 5 through-flow periods.

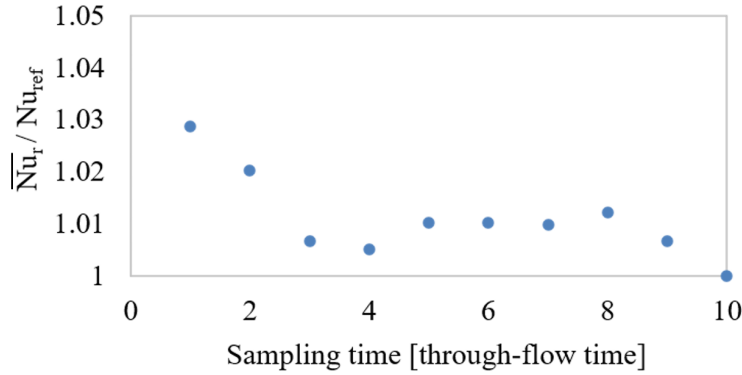


Fig. 12: Sampling time length study. The reference value  $Nu_{ref}$  is  $\overline{Nu}_r$  after sampling for 10 through-flow times

## 4.2 Laminar flow results

In the present section, several wall temperatures are tested for the same Reynolds number ( $Re_r=720$ ). A quasi-adiabatic case ( $TR=0.98$ ) is used as the reference, since the Reynolds analogy might not be suitable to calculate the reference Nusselt number for this kind of geometry.

### 4.2.1 Local Reynolds number effect

Similarly to the flat plate boundary layer analysis illustrated in figs. 6 and 7, the influence of wall temperature on  $Re_{local}$  for an array of surface microstructures is first examined. In particular, the difference in  $Re_{local}(x,y)$  between  $TR=0.5$  and the reference quasi-adiabatic case ( $TR=0.98$ ) is depicted on an xy-plane taken at  $z=0$  (mid-plane cut). For the given  $z$  value, the definitions for the local Re differences introduced in eq. (3) can be adapted as described in eq. (4).

$$\begin{aligned}
 D_{tot}(x,y) &= \frac{Re_{local}(x,y)_{TR05} - Re_{local}(x,y)_{TR098}}{Re_{local}(x,y)_{TR098}} \\
 D_u(x,y) &= \frac{\frac{\rho(x,y)_{TR098} u(x,y)_{TR05} r}{\mu(x,y)_{TR098}} - Re_{local}(x,y)_{TR098}}{Re_{local}(x,y)_{TR098}} \\
 D_p(x,y) &= \frac{\frac{\rho(x,y)_{TR05} u(x,y)_{TR098} r}{\mu(x,y)_{TR098}} - Re_{local}(x,y)_{TR098}}{Re_{local}(x,y)_{TR098}} \\
 D_\mu(x,y) &= \frac{\frac{\rho(x,y)_{TR098} u(x,y)_{TR098} r}{\mu(x,y)_{TR05}} - Re_{local}(x,y)_{TR098}}{Re_{local}(x,y)_{TR098}}
 \end{aligned} \tag{4}$$

The total changes in the local Reynolds number,  $D_{tot}$ , caused by TR variations are plotted in fig. 13. Wall cooling substantially increases  $Re_{local}$  near the surface microstructure array, showing an overall consistent picture with that of a flat plate boundary layer in fig. 6. Nevertheless, a significant difference is observed in the upper part of the recirculation regions, where negative  $D_{tot}$  values are detected locally (region indicated with 'A' in fig. 13).

The individual contributions of local velocity, density, and dynamic viscosity, to the  $Re_{local}$  variation, are depicted in fig. 14. In line with the flat plate boundary layer analysis, both local density, and dynamic viscosity contribute to increase the local Reynolds number, and local density shows a more marked impact than dynamic viscosity (fig. 14b-c). On the other hand, the behavior of local velocity (fig. 14a) differs significantly from the flat plate case, resulting in negative  $D_u$  values in the separation regions (area indicated with 'A' in fig. 14a). The results in fig. 14 suggest that local velocity is responsible for the negative  $D_{tot}$  regions illustrated in fig. 13.

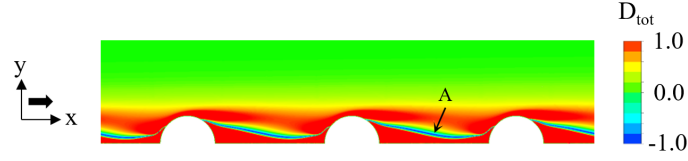


Fig. 13: Impact of  $TR=0.5$  on  $Re_{local}$  for an array of surface microstructures

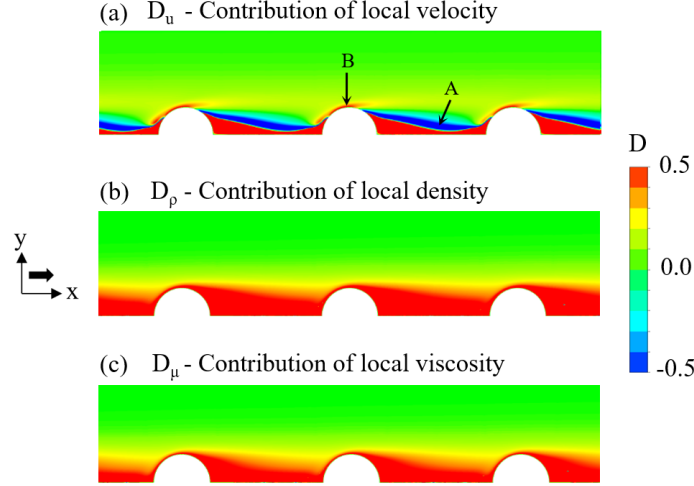


Fig. 14: The contribution of velocity, dynamic viscosity and density to increasing  $Re_{local}$  in the near wall region for  $TR=0.5$

To understand why the contribution of local velocity  $D_u$  differs significantly between a flat plate boundary layer and a surface microstructure array, the impact of TR on the velocity field on a midcut-plane ( $z=0$ ) is shown in fig. 15. Wall cooling ( $TR=0.5$ ) increases the near wall density resulting in higher local fluid inertia, and delayed reattachment. Inversely, in the heated wall case ( $TR=1.5$ ), reduced near-wall density corresponds to an earlier flow reattachment. Therefore, the wall cooling is seen to increase the size of the recirculation zone, and vice versa for the wall heating.

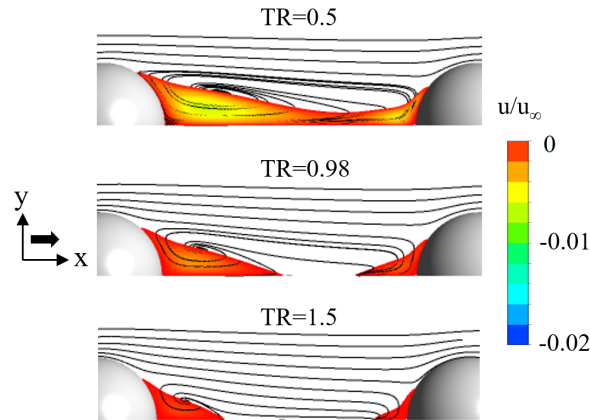


Fig. 15: Impact of TR on the velocity field near surface microstructures. The contour is clipped at  $u/u_\infty=0$ , thus reversed flow only is depicted

Differently from that observed for a flat plate boundary layer, where no flow separation takes place, in the case of hemispherical microstructures, the  $D_u$  contour (fig. 14a) is influenced by the shape and size of the recirculation region which is dependent on TR. The enlarged separation of the cooled wall case ( $TR=0.5$ ) corresponds to a local region ('A' in fig. 14a) where the velocity is lower compared to the adiabatic reference case. Consequently, a significant local negative contribution from the velocity changes to the local Reynolds number is illustrated in fig. 14a. On the other hand, similarly to the flat plate

boundary layer (fig. 4), the frontal surface attached boundary layer (marked as 'B' in fig. 14a) shows higher local velocity for the cooled wall case. Rather contrasting velocity contributions around the flow separation over the hemisphere surface are observed: there is a positive contribution of the frontal part where the boundary layer is attached, but the contribution becomes sharply negative right after the separation.

The same study is carried out for the heated wall case ( $TR=1.5$ ). Consistently with the flat plate boundary layer findings (fig. 6), the near-wall  $Re_{local}$  values show an overall reduction due to wall heating, as indicated in fig. 16. Meanwhile, a significant difference is detected in the recirculation region, where  $D_{tot}$  reaches positive values in 'A' (flipped compared to  $TR=0.5$ ).

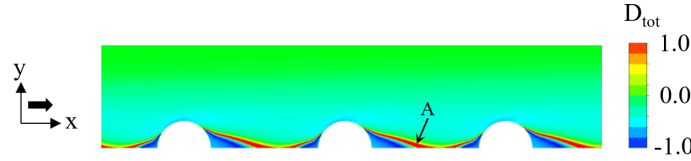


Fig. 16: Impact of  $TR=1.5$  on  $Re_{local}$  for an array of surface microstructures

The individual contributions of local velocity, density, and dynamic viscosity, to the  $Re_{local}$  variation for  $TR=1.5$ , are depicted in fig. 17. The reduced separation region in the heated wall case translates into higher local velocity in the upper part of the recirculation areas ('A' in fig. 17a), and is responsible for the  $D_{tot} > 0$  regions indicated with 'A' in fig. 16.

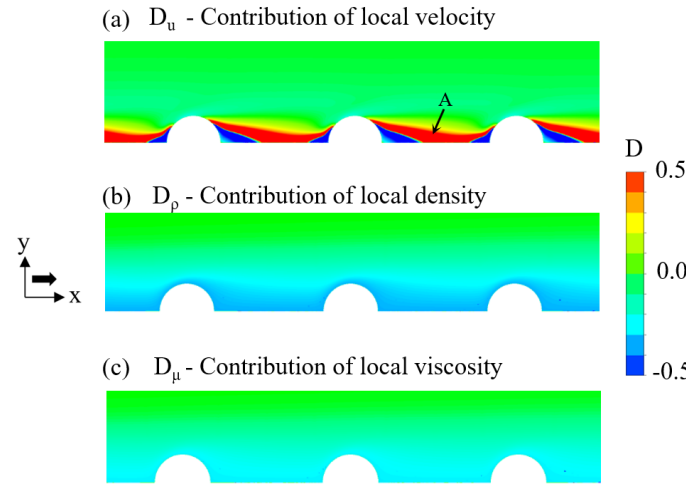


Fig. 17: The contribution of velocity, dynamic viscosity and density to reducing  $Re_{local}$  in the near wall region for  $TR=1.5$

#### 4.2.2 Impact of TR on aerothermal parameters

The influence of TR on performance parameters for an array of hemispheric surface microstructures in the laminar regime ( $Re_r=720$ ) is studied in this section. The variation of Nusselt number ( $Nu_r$ ) due to heat transfer, is illustrated in fig. 18a, showing that Nusselt number increases as the local Reynolds number grows (high near-wall  $Re_{local}$  for  $TR=0.5$ , see fig. 13). In comparison with the flat plate boundary layer where the impact of TR on performance parameters is negligible (see table 1), wall cooling ( $TR=0.5$ ) increases  $Nu_r$  by  $\sim 15\%$ .

The influence of TR on the drag coefficient is depicted in fig. 18b. In contrast with Nusselt number, the total drag coefficient  $C_D$  increases by  $\sim 15\%$  for the heated wall case. Differently from that observed for a flat plate boundary layer where the frictional drag coefficient is largely unchanged for different TR values (see table 1), for a surface microstructure array, wall temperature has a significant impact on  $C_{Df}$ .

Our attention is brought to the opposite variations of friction and pressure drag components at different TRs. As shown in fig. 18b, for a cooled wall ( $TR=0.5$ ), the frictional drag is lower than the pressure drag, but the opposite is observed for a heated wall ( $TR=1.5$ ). To help interpret the relatively decreased frictional drag for a cooled wall, we examine the local

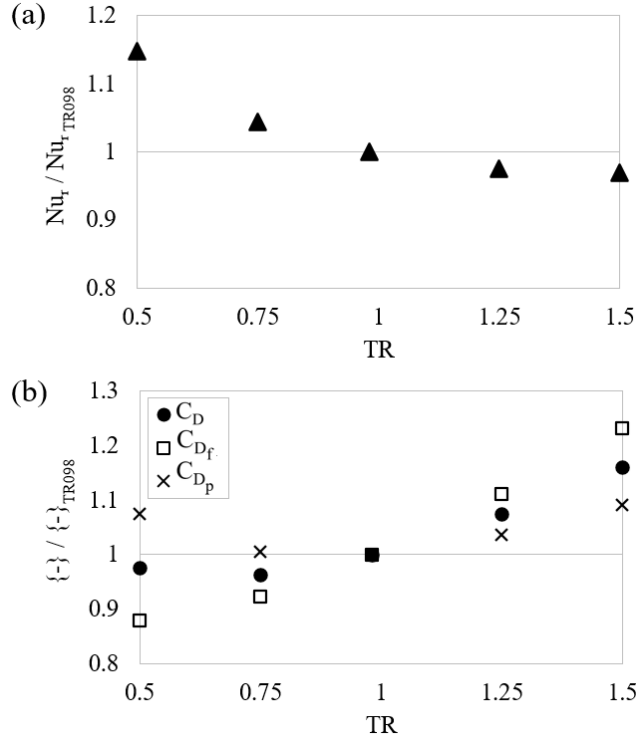


Fig. 18: Impact of TR on aerothermal parameters

friction coefficient contours over the hemisphere surface at  $TR=0.5$  and  $TR=1.5$  as shown in fig. 19. The major changes happen strikingly in the local area around the flow separation. The bulk frontal surface area until separation seems to have largely negligible changes, similarly to the flat plate boundary layer, subject to the compensating effects between viscosity and velocity gradient (as discussed in section 3.2). On the other hand, the compensating mechanism stops functioning in the rear part of the microstructure in the proximity of the separation line (blue stripe indicated with 'A' in fig. 19a, red stripe indicated with 'B' in fig. 19b). For  $TR=0.5$ , the earlier separation leads to lower local velocity gradient in the separated region while dynamic viscosity is also lower compared to the quasi-adiabatic case, resulting in much lower local shear stress. Inversely, wall heating ( $TR=1.5$ ) causes higher local velocity gradient due to postponed separation and higher near-wall dynamic viscosity due to the heating, leading to a much higher shear stress than the reference case. The impact of TR on the frictional drag coefficient is smaller for  $TR=0.5$  than it is for  $TR=1.5$  due to the size of the 'A' area, which is smaller than the 'B' area (fig. 19).

The relatively increased pressure drag at a cooled wall condition ( $TR=0.5$ ) depicted in fig. 18b can be easily attributed to the enlarged recirculation due to the wall cooling (fig. 15). A rather contradicting behavior is observed for the heated wall case ( $TR=1.5$ ), where the pressure drag coefficient is seemingly higher compared to the quasi-adiabatic solution. This is likely to be caused by the increased frontal stagnation effect due to the reduced separation of the upstream microstructure element (e.g. comparing the frontal streamlines and flow patterns between fig. 19a and fig. 19b).

The interdependence between aerodynamics and heat transfer, for an array of surface microstructures in the laminar regime, translates into a more significant impact on performance parameters compared to a flat plate boundary layer. Next, we will discuss the consequences of the substantial local Reynolds number variation and its impact on turbulent transition for the same array of hemispheric microstructures.

#### 4.3 Transition to turbulent flow

The significant variation of  $Re_{local}$  does beg a question: how would turbulent transition behave under the influence of wall heat transfer? In general, the impact of wall thermal boundary condition (BC) on transition seems to lack consistent observations and understanding, as commented in the introduction. Furthermore, there seem to be hardly any previous findings for micro-structured surfaces in particular.

In this section, we address this question in three subsections: i) the transitional behavior under heat transfer influence at a given transitional  $Re_r$ ; ii) the transition characteristics, in terms of the overall aerothermal parameters ( $C_D$ ,  $Nu$ ), for a range of  $Re_r$  values, in addition to the applicability of the incompressible model in predicting such transitional behavior; and iii) a more unified non-dimensional characterization of the transitional regime to account for TR effects.

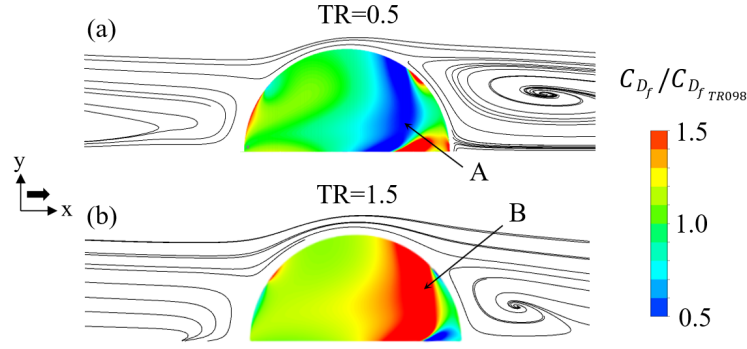


Fig. 19: Impact of TR on the local  $C_{Df}$  distribution. The  $C_{Df}$  contour is 3D, and 2D streamlines are plotted on the mid-pitch cut-plane ( $z=0$ )

#### 4.3.1 Transitional flow behavior at a given $Re_r$

The flow fields at  $Re_r=4000$  for two different TR values are illustrated in fig. 20. The quasi-adiabatic case shows a laminar flow field as depicted in fig. 20a, whereas, the cooled wall case ( $TR=0.5$ ) is characterized by unsteady separated flow as illustrated in fig. 20b. The increased local velocity in the shear layer at  $TR=0.5$  (area indicated with 'B' in fig. 14a) makes the flow field more prone to shear layer instabilities. Such a finding is in line with the substantially higher local Reynolds number near the microstructures shown for  $TR=0.5$  in fig. 13.

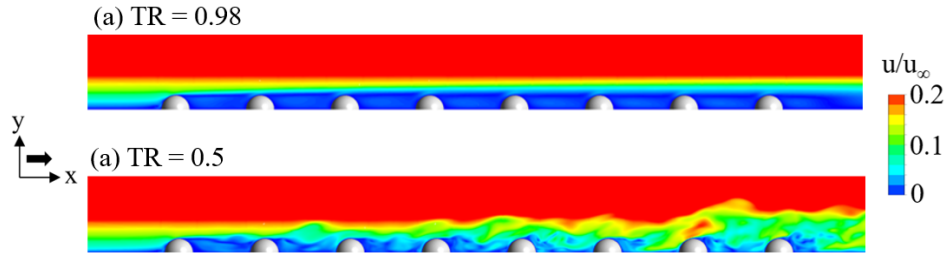


Fig. 20: Velocity field at  $Re_r=4000$ . a)  $TR=0.98$ , b)  $TR=0.5$

To further assess the cooling induced unstable flow, we examine the power spectral density in a position where the flow is more developed. The axial velocity spectrum at a point downstream of the last microstructure for the cooled wall case ( $TR=0.5$ ) at  $Re_r=4000$  is illustrated in fig. 21, showing a spectrum similar to a typical turbulent one albeit not being fully developed. We therefore observe a clear promotion of turbulent transition for the cooled wall case, which is in line with the substantial increase of the local Reynolds number as established in the previous sections.

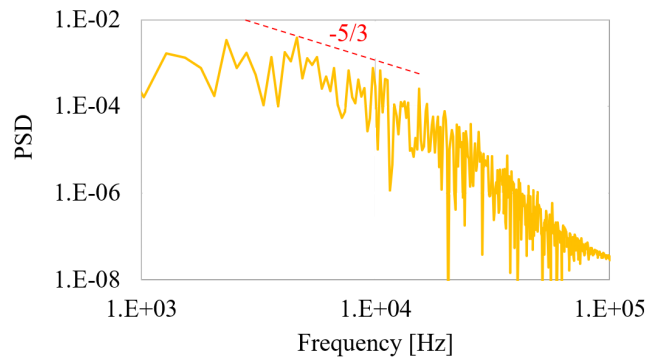


Fig. 21: Power spectral density of axial velocity downstream of the last microstructure at  $Re_r = 4000$  for  $TR=0.5$

### 4.3.2 Transitional regime at different $Re_r$

We now analyse the flows for various  $Re_r$ , ranging from laminar to turbulent flows, at three wall temperatures:  $TR=0.5$  (cooled wall),  $TR=0.98$  (quasi-adiabatic), and  $TR=1.5$  (heated wall). Performance parameters are area-averaged over microstructures number 5, 6, and 7 of the row (see fig. 9) to better represent a more fully developed flow.

The drag coefficient is shown for several Reynolds number values ( $Re_r$ ) in fig. 22. In the quasi-adiabatic case ( $TR=0.98$ ), turbulent transition takes place at  $Re_r \sim 5000$ , whereas for  $TR=0.5$  and  $TR=1.5$ , it occurs respectively at  $Re_r \sim 2500$  and  $Re_r \sim 7500$ . These preliminary results suggest that the critical Reynolds number drops by 50% for  $TR=0.5$ , and increases by 50% for  $TR=1.5$ , indicating that TR has a substantial impact on transition given the corresponding substantial change in  $Re_{local}$ .

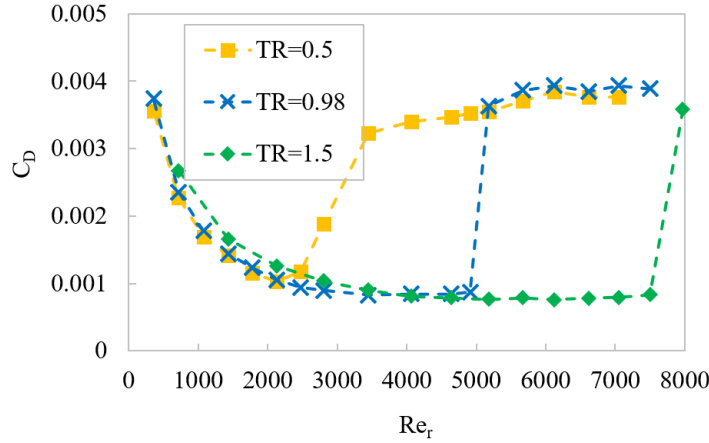


Fig. 22:  $C_D$ - $Re_r$  chart for three wall temperatures: cooled wall ( $TR=0.5$ ), quasi-adiabatic ( $TR=0.98$ ), and  $TR=1.5$  (heated wall)

Similarly, Nusselt number with its wall temperature dependency is depicted in fig. 23. For  $Re_r < 2500$ , the results under all TR conditions are laminar, and  $Nu_{rTR05} \sim 1.1Nu_{rTR098}$ . On the other hand, for  $Re_r > 7500$ , all the wall temperatures tested lead to turbulent flows.

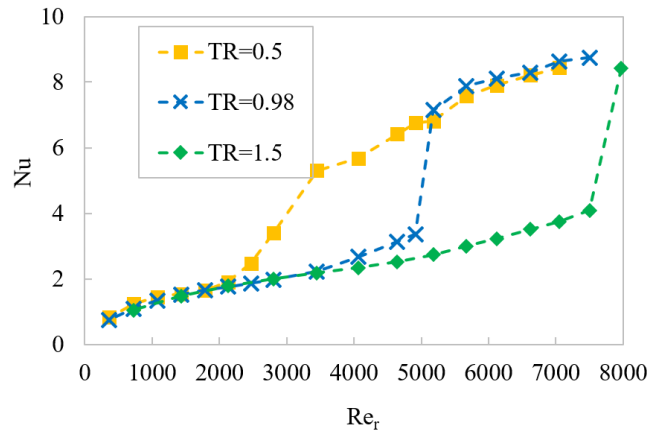


Fig. 23:  $Nu_r$ - $Re_r$  chart for three wall temperatures: cooled wall ( $TR=0.5$ ), quasi-adiabatic ( $TR=0.98$ ), and  $TR=1.5$  (heated wall)

Another indication of a more fully-developed turbulent flow for  $Re_r > 5000$  at  $TR=0.5$  and  $TR=0.98$  is provided by the axial velocity spectrum taken at a point downstream of the last microstructure. For both TR values the standard -5/3 distribution is detected in the inertia scale range of the spectra, as illustrated in fig. 24.

Turbulence intensity is evaluated at the same point used for the velocity spectrum, indicating that  $TR=0.5$  results in a slightly higher turbulence intensity than the reference quasi-adiabatic case as shown in table 4.

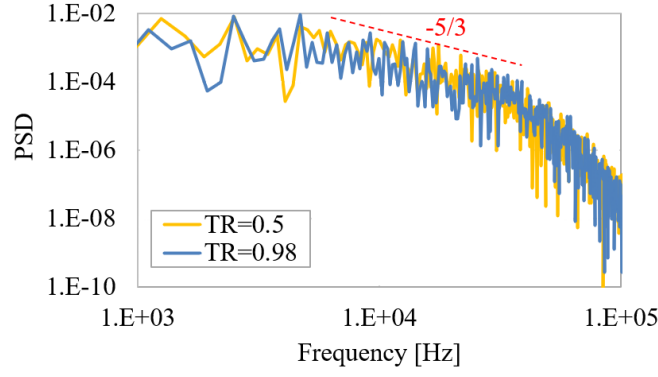


Fig. 24: Power spectral density of axial velocity downstream of the last microstructure at  $Re_r = 6200$  for  $TR=0.5$ , and  $TR=0.98$

Table 4: Turbulence intensity

$TR$	$I$
0.5	0.246
0.98	0.230

To illustrate the effect of  $TR$  on the separation regions in the turbulent regime, the time-averaged velocity field at  $Re_r=6200$  is depicted in fig. 25. In contrast with the laminar regime, where the cooled wall case ( $TR=0.5$ ) presents a larger recirculation region (fig. 15), for the turbulent flow regime,  $TR=0.5$  shows a delayed separation and smaller recirculation region. Bearing in mind the earlier transition with the cooled wall, we would expect that the corresponding turbulent flow in this case is more fully developed than that for the quasi-adiabatic  $TR$ , as indicated by the corresponding turbulence intensities (table 4). As such, a stronger turbulent mixing in the near wall region might lead to a delayed separation for the cooled case as seen in fig. 25.

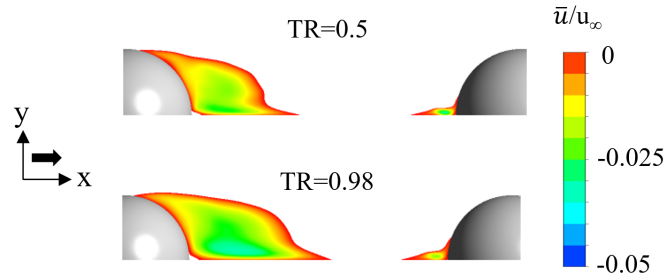


Fig. 25: Time-averaged velocity,  $Re_r=6200$ . The velocity contour is clipped at  $\bar{u}/u_\infty=0$

A relevant modelling issue of interest, particularly in the context of predicting transition under the influence of heat transfer, is the applicability of the incompressible flow model. Incompressible flow assumptions are often adopted for transition studies. Therefore, a question arises: can the incompressible flow model predict the transition behavior under the influence of heat transfer? The flow field obtained using the incompressible flow model is compared with the compressible results in fig. 26 for the same Reynolds number ( $Re_r=3450$ ). For the incompressible simulations (fig. 26b), fluid properties are fixed at  $T=(T_{01} - T_w)/2$ , and  $u_\infty$  is adjusted to match the prescribed  $Re_r$ .

In the present study, the incompressible flow model results are shown to be completely unable to capture the  $TR$  influence. The Nusselt number variation with  $Re_r$  predicted by the incompressible flow at  $TR=0.5$  is almost the same as that predicted by the compressible flow model at  $TR=0.98$ , as shown in fig. 27. In fact, in an incompressible flow, the velocity field can be obtained by solving only the continuity and momentum equations. The energy equation is effectively redundant as far as the velocity field is concerned, thus the temperature field is passive and has no effect on the velocity field. Those



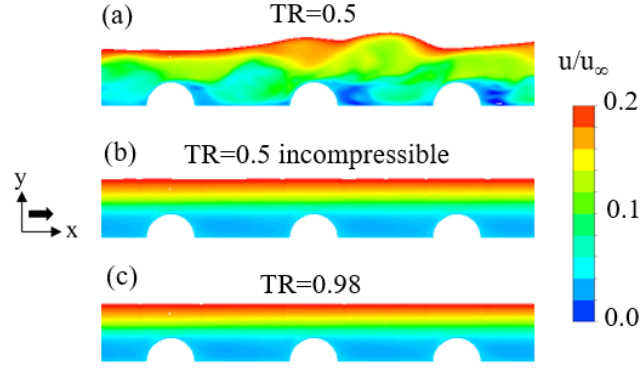


Fig. 26: Velocity contours at  $Re_r=3450$ . a) Compressible flow at  $TR=0.5$ ; b) Incompressible flow at  $TR=0.5$ ; c) Compressible flow at  $TR=0.98$

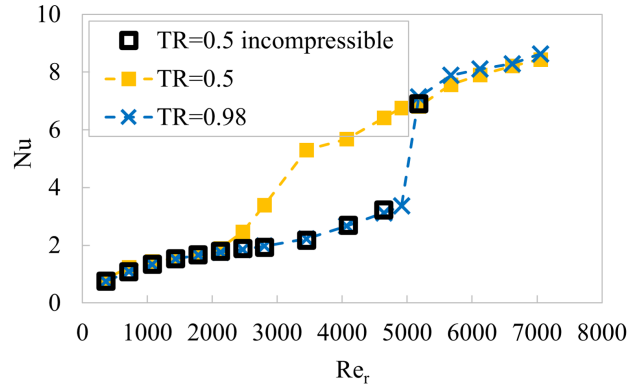


Fig. 27: Applicability of the incompressible flow solution to transition under the influence of heat transfer

results suggest that the incompressible flow model is unable to predict the interplay between aerodynamics and heat transfer, manifested in terms of the influence of TR on laminar-turbulent transition for the microstructured surface.

#### 4.3.3 Non-dimensional characterization

Conventionally, the key non-dimensional aerothermal parameters ( $C_D, Nu$ ) are considered to be only dependent on  $Re$  (for a given geometry configuration). On the other hand, in the present study, we observe different aerothermal characteristics for different TRs, as shown in figs. 22 and 23. For more general characterization and efficient applications to different wall temperature conditions, we thus ask, is there a new independent parameter or a non-dimensional group so that a unified characteristic relation can be established to automatically take into account the TR effect?

If we consider Mach number effects to be negligible for such low speed flows, the conventional non-dimensional groups  $C_f$  and  $Nu$  only depend on Reynolds number and Prandtl number. For typical aerothermal analyses (viscous flow and convective heat transfer), non-dimensional performance parameters are commonly expressed in a power index form:

$$(C_f, Nu) = C Pr^n Re^m \quad (5)$$

where  $C$ ,  $m$ ,  $n$  are constants depending on geometry configurations and flow conditions. In the present work, the emphasis is placed on the wall heat transfer effect marked by different temperature ratios (TRs). Therefore, extra attention has been directed to the additional non-dimensional group (TR), which is included as follows:

$$(C_f, Nu) = C Pr^n Re^m TR^k \quad (6)$$

For a given fluid,  $Pr$  is constant, thus its influence can simply be included in constant  $C$ , i.e.:

$$(C_f, Nu) = C Re^m TR^k \quad (7)$$

Equation (7) translates into the following relations for  $C_f$  and  $Nu$  with the corresponding set of constant indices:

$$\begin{aligned} C_f TR^{z_{C_f}} &= C_{C_f} Re^{m_{C_f}} \\ Nu TR^{z_{Nu}} &= C_{Nu} Re^{m_{Nu}} \end{aligned} \quad (8)$$

Equation (8) can also be rewritten in the following general functional relations:

$$\begin{aligned} C_f TR^{z_{C_f}} &= f_1(Re) \\ Nu TR^{z_{Nu}} &= f_2(Re) \end{aligned} \quad (9)$$

The above eqs. (8) and (9) imply that when seeking a unified Reynolds number correlation for different TRs, we should consider using the groups  $C_f TR^{z_{C_f}}$  and  $Nu TR^{z_{Nu}}$ . The implementation of the new grouping requires to determine the constants  $z_{C_f}$  and  $z_{Nu}$ . Considering the rather different aerothermal characteristics at different Reynolds, we will have to determine the constants separately for different parts of a transition process. Taking the cooled wall case as an example, the characteristics for the whole  $Re$  range can be typically divided into four parts: laminar (I), transitional due to cooling (II), transitioned due to cooling (III), and turbulent (IV), as shown in fig. 28. The corresponding constants can be fixed by given solutions for each part respectively. The results for  $Nu$  and  $C_D$  with the new non-dimensional grouping are shown in fig. 29. We can see that the three curves for three TRs are now collapsed into one for both  $C_D$  and  $Nu$ , as intended.

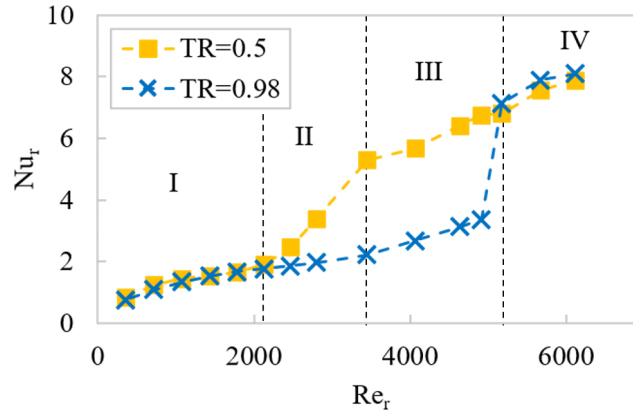


Fig. 28: Non-dimensional analysis method to determine  $z_{Nu}$

## 5 Summary and Conclusions

Enhanced understanding and prediction of aerodynamics and convective heat transfer characteristics for surface microstructures have been continuously pursued, and are further motivated by the rapid development of AM technologies in recent years. In the context of aerothermal design and management of high temperature components, convective heat transfer is typically regarded as predominantly driven by fluid flow. An issue of interest is the interaction between the heat transfer and the flow field, and more specifically, if and how heat transfer may affect the flow field. In the present work, a systematic computational study is carried out for two contrasting configurations (a flat plate boundary layer and an array of hemispheric micro-structures) at three wall-inflow temperature ratio (TR) values: cooled ( $TR=0.5$ ), adiabatic ( $TR=1$ ) and heated wall ( $TR=1.5$ ). The following concluding observations and comments can be made.

The basic validation and sensitivity studies are conducted for a flat plate laminar boundary layer. At first, a seemingly contradicting observation is made: common aerothermal parameters  $C_f$  and  $Nu$  appear largely insensitive to the wall heat transfer, but the velocity profiles are substantially affected by TR. It turns out that a compensating effect is at play between fluid viscosity and velocity gradient in the boundary layer, leading to the heat transfer influence on the flow being largely ‘masked’ if judged merely based on  $C_f$  and  $Nu$ . This finding prompts the authors to explore the local Reynolds number as a more useful indicator for the influence of heat transfer on the flow field.

It is further observed and backed up by a detailed examination of the contributions to the local Reynolds number from each fluid property or flow variable, that a cooled wall leads to a very significant increase in the local Reynolds number

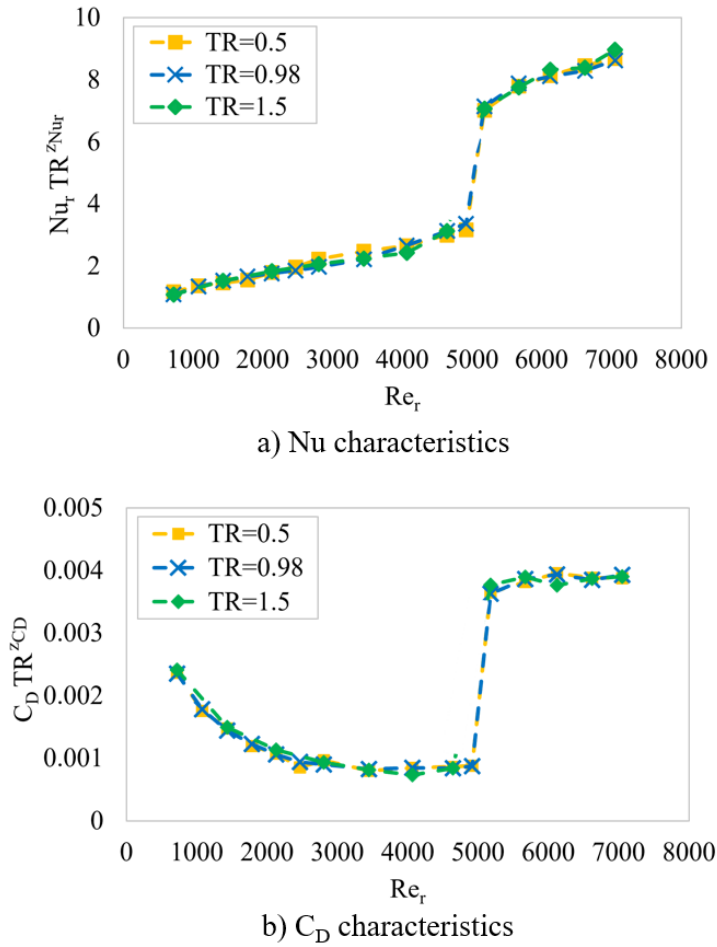


Fig. 29: Regrouped non-dimensional characteristics

within the boundary layer. For the microstructures, the local velocity distributions around the flow separations and in the recirculation zones cause distinctive local variations of the local Reynolds number, directly attributable to the changes in flow separation with notable associated changes in drag and heat transfer.

More remarkably, in line with the substantial increase of the local Reynolds number for the micro-structures under wall cooling, a much earlier transition to a turbulent flow is predicted by the scale-resolving LES simulations. The corresponding bulk-flow critical Reynolds number, for the cooled wall case, is reduced by about 50%, and increased by about 50% for the heated wall. It is also demonstrated by a comparative test that the incompressible flow LES solutions under the cooling condition ( $TR=0.5$ ) produce almost the same results as the compressible flow solutions at the near-adiabatic condition ( $TR \sim 1$ ). Thus, an incompressible flow model is deemed to be unsuitable for transition predictions if there are significant heat transfer effects as in the present cases.

Further considerations are given to a more unified characterization for scaling wall heat transfer effects in practical applications. A regrouping of the non-dimensional parameters ( $C_D$ ,  $Nu$ ) with  $TR$  is proposed. With the new regrouping, the non-dimensional aerothermal performance results with different  $TR$ s can now be collapsed into a single curve with regard to Reynolds number, which, once established, may be simply used to get the aerothermal performance results at different  $TR$ s at no extra cost.

## Acknowledgements

The work is sponsored jointly by EPSRC CDT in Gas Turbine Aerodynamics and Siemens Energy. The authors are grateful to Roger Wells, Yansheng Li, and Omar Valero for the valuable technical discussions. The authors would also like to acknowledge the use of the University of Oxford Advanced Research Computing (ARC) facility in carrying out this work. <http://dx.doi.org/10.5281/zenodo.22558>

This research was funded in part by UK EPSRC [EP/L015943/1]. For the purpose of Open Access, the authors have applied a CC BY public copyright licence to any Author Accepted Manuscript (AAM) version arising from this submission.

## List of tables

Table 1.	Impact of TR on performance parameters . . . . .	6
Table 2.	Mesh size sensitivity . . . . .	9
Table 3.	Time step size sensitivity . . . . .	9
Table 4.	Turbulence intensity . . . . .	16

## List of figures

Figure 1.	Flat plate boundary layer domain (height and length are to the scale $H/L=2.5$ ). . . . .	4
Figure 2.	Surface microstructure array domain: a row of eight hemispherical surface microstructures of $500\mu m$ radius . . . . .	4
Figure 3.	Mesh dependency study for flat plate boundary layer . . . . .	5
Figure 4.	Impact of TR on the velocity profile . . . . .	5
Figure 5.	Profiles of dynamic viscosity and velocity gradient at different wall temperature conditions non-dimensionalized using adiabatic values at the wall . . . . .	6
Figure 6.	Local Reynolds number profile . . . . .	7
Figure 7.	The contribution of velocity, dynamic viscosity, and density to increasing $Re_{local}$ in the near-wall region for $TR=0.5$ . . . . .	8
Figure 8.	Inlet velocity profile, obtained by specifying a total pressure profile to match the laminar Blasius solution as shown . . . . .	8
Figure 9.	Velocity contours, a) Laminar flow field $Re_r=700$ , b) Turbulent flow field $Re_r=6200$ . . . . .	8
Figure 10.	Vorticity iso-surfaces colored with $u$ values: a) laminar, b) turbulent . . . . .	9
Figure 11.	O-grid mesh around one of the microstructures . . . . .	9
Figure 12.	Sampling time length study. The reference value $Nu_{ref}$ is $\overline{Nu_r}$ after sampling for 10 through-flow times . . . . .	10
Figure 13.	Impact of $TR=0.5$ on $Re_{local}$ for an array of surface microstructures . . . . .	11
Figure 14.	The contribution of velocity, dynamic viscosity and density to increasing $Re_{local}$ in the near wall region for $TR=0.5$ . . . . .	11
Figure 15.	Impact of TR on the velocity field near surface microstructures. The contour is clipped at $u/u_\infty=0$ , thus reversed flow only is depicted . . . . .	11
Figure 16.	Impact of $TR=1.5$ on $Re_{local}$ for an array of surface microstructures . . . . .	12
Figure 17.	The contribution of velocity, dynamic viscosity and density to reducing $Re_{local}$ in the near wall region for $TR=1.5$ . . . . .	12
Figure 18.	Impact of TR on aerothermal parameters . . . . .	13
Figure 19.	Impact of TR on the local $C_{Df}$ distribution. The $C_{Df}$ contour is 3D, and 2D streamlines are plotted on the mid-pitch cut-plane ( $z=0$ ) . . . . .	14
Figure 20.	Velocity field at $Re_r=4000$ . a) $TR=0.98$ , b) $TR=0.5$ . . . . .	14
Figure 21.	Power spectral density of axial velocity downstream of the last microstructure at $Re_r = 4000$ for $TR=0.5$ . . . . .	14
Figure 22.	$C_D-Re_r$ chart for three wall temperatures: cooled wall ( $TR=0.5$ ), quasi-adiabatic ( $TR=0.98$ ), and $TR=1.5$ (heated wall) . . . . .	15
Figure 23.	$Nu_r-Re_r$ chart for three wall temperatures: cooled wall ( $TR=0.5$ ), quasi-adiabatic ( $TR=0.98$ ), and $TR=1.5$ (heated wall) . . . . .	15
Figure 24.	Power spectral density of axial velocity downstream of the last microstructure at $Re_r = 6200$ for $TR=0.5$ , and $TR=0.98$ . . . . .	16
Figure 25.	Time-averaged velocity, $Re_r=6200$ . The velocity contour is clipped at $\bar{u}/u_\infty=0$ . . . . .	16
Figure 26.	Velocity contours at $Re_r=3450$ . a) Compressible flow at $TR=0.5$ ; b) Incompressible flow at $TR=0.5$ ; c) Compressible flow at $TR=0.98$ . . . . .	17
Figure 27.	Applicability of the incompressible flow solution to transition under the influence of heat transfer . . . . .	17
Figure 28.	Non-dimensional analysis method to determine $z_{Nu}$ . . . . .	18
Figure 29.	Regrouped non-dimensional characteristics . . . . .	19

## References

- [1] Yaras, M. I., 2004. "Measurements of Surface-Roughness Effects on the Development of a Vortex Produced by an Inclined Jet in Cross-Flow". *Journal of Fluids Engineering*, **126**(3), 07, pp. 346–354.
- [2] Tachie, M. F., Bergstrom, D. J., and Balachandar, R., 2005. "Roughness Effects on the Mixing Properties in Open Channel Turbulent Boundary Layers". *Journal of Fluids Engineering*, **126**(6), 03, pp. 1025–1032.
- [3] Shin, J. H., and Jin Song, S., 2014. "Pressure Gradient Effects on Smooth and Rough Surface Turbulent Boundary Layers—Part I: Favorable Pressure Gradient". *Journal of Fluids Engineering*, **137**(1), 09, 011203.
- [4] Shin, J. H., and Jin Song, S., 2014. "Pressure Gradient Effects on Smooth- and Rough-Surface Turbulent Boundary Layers—Part II: Adverse Pressure Gradient". *Journal of Fluids Engineering*, **137**(1), 09, 011204.
- [5] Rostamy, N., Bergstrom, D. J., Sumner, D., and Bugg, J. D., 2011. "An Experimental Study of a Turbulent Wall Jet on Smooth and Transitionally Rough Surfaces". *Journal of Fluids Engineering*, **133**(11), 11, 111207.
- [6] Goodhand, M. N., and Miller, R. J., 2011. "The Impact of Real Geometries on Three-Dimensional Separations in Compressors". *Journal of Turbomachinery*, **134**(2), 06, 021007.
- [7] Yan, H., Zhang, W.-M., Peng, Z.-K., and Meng, G., 2015. "Effect of Three-Dimensional Surface Topography on Gas Flow in Rough Micronozzles". *Journal of Fluids Engineering*, **137**(5), 05, 051202.
- [8] Jeong, H., and Song, S. J., 2021. "Surface Roughness Impact on Boundary Layer Transition and Loss Mechanisms Over a Flat-Plate Under a Low-Pressure Turbine Pressure Gradient". *Journal of Turbomachinery*, **144**(1), 09, 011005.
- [9] Bogard, D. G., Schmidt, D. L., and Tabbita, M., 1998. "Characterization and Laboratory Simulation of Turbine Airfoil Surface Roughness and Associated Heat Transfer". *Journal of Turbomachinery*, **120**(2), 04, pp. 337–342.
- [10] Sigal, A., and Danberg, J. E., 1990. "New correlation of roughness density effect on the turbulent boundary layer". *Journal of Turbomachinery*, **28**(3), pp. 554–556.
- [11] Waigh, D., and Kind, R. J., 1998. "Improved aerodynamic characterization of regular three-dimensional roughness". *AIAA Journal*, **36**(6), p. 1117–1119.
- [12] Stripf, M., Schulz, A., and Wittig, S., 2005. "Surface Roughness Effects on External Heat Transfer of a HP Turbine Vane". *Journal of Turbomachinery*, **127**(1), 02, pp. 200–208.
- [13] Bons, J. P., 2010. "A Review of Surface Roughness Effects in Gas Turbines". *Journal of Turbomachinery*, **132**(2), 01, 021004.
- [14] Chatzikyriakou, D., Buongiorno, J., Caviezel, D., and Lakehal, D., 2015. "Dns and les of turbulent flow in a closed channel featuring a pattern of hemispherical roughness elements". *International Journal of Heat and Fluid Flow*, **53**, pp. 29 – 43.
- [15] Gramespacher, C., Stripf, M., and Bauer, H.-J., 2021. "The Influence of Deterministic Surface Roughness and Freestream Turbulence on Transitional Boundary Layers: Heat Transfer Distributions and a New Transition Onset Correlation". *Journal of Turbomachinery*, **144**(4), 11, 041001.
- [16] Goodhand, M. N., Walton, K., Blunt, L., Lung, H. W., Miller, R. J., and Marsden, R., 2016. "The Limitations of Using "Ra" to Describe Surface Roughness". *Journal of Turbomachinery*, **138**(10), 04, 101003.
- [17] Kapsis, M., and He, L., 2018. "Analysis of Aerothermal Characteristics of Surface Microstructures". *Journal of Fluids Engineering*, **140**(5), 01, 051104.
- [18] Stimpson, C. K., Snyder, J. C., Thole, K. A., and Mongillo, D., 2016. "Roughness Effects on Flow and Heat Transfer for Additively Manufactured Channels". *Journal of Turbomachinery*, **138**(5), 01, 051008.
- [19] Kirsch, K. L., and Thole, K. A., 2017. "Pressure loss and heat transfer performance for additively and conventionally manufactured pin fin arrays". *International Journal of Heat and Mass Transfer*, **108**, pp. 2502 – 2513.
- [20] Ferster, K. K., Kirsch, K. L., and Thole, K. A., 2017. "Effects of Geometry, Spacing, and Number of Pin Fins in Additively Manufactured Microchannel Pin Fin Arrays". *Journal of Turbomachinery*, **140**(1), 10, 011007.
- [21] Chu, K.-H., Enright, R., and Wang, E. N., 2012. "Structured surfaces for enhanced pool boiling heat transfer". *Applied Physics Letters*, **100**(24), June, p. 241603.
- [22] Miao, X., Zhang, Q., Atkin, C., Sun, Z., and Li, Y., 2018. "Improving Purge Air Cooling Effectiveness by Engineered End-Wall Surface Structures—Part I: Duct Flow". *Journal of Turbomachinery*, **140**(9), 08, 091001.
- [23] Jenny, P., Lee, S., and Tchelepi, H., 2003. "Multi-scale finite-volume method for elliptic problems in subsurface flow simulation". *Journal of Computational Physics*, **187**(1), p. 47–67.
- [24] Errera, M.-P., and Turpin, G., 2013. "Temporal multiscale strategies for conjugate heat transfer problems". *Journal of Coupled Systems and Multiscale Dynamics*, **1**(1), p. 89–98.
- [25] He, L., 2018. "Multiscale block spectral solution for unsteady flows". *International Journal for Numerical Methods in Fluids*, **86**(10), pp. 655–678.
- [26] Kapsis, M., He, L., Li, Y. S., Valero, O., Wells, R., Krishnababu, S., Gupta, G., Kapat, J., and Schaefer, M., 2020. "Multiscale Parallelized Computational Fluid Dynamics Modeling Toward Resolving Manufacturable Roughness". *Journal of Engineering for Gas Turbines and Power*, **142**(2), 12, 021001.
- [27] Moffat, R. J., 1998. "What's new in convective heat transfer?". *International Journal of Heat and Fluid Flow*, **19**(2), pp. 90–101.

- [28] Fitt, A., Forth, C., Robertson, B., and Jones, T., 1986. "Temperature ratio effects in compressible turbulent boundary layers". *International Journal of Heat and Mass Transfer*, **29**(1), pp. 159–164.
- [29] Kays, W. M., 2011. *Convective heat and mass transfer*. Tata McGraw-Hill Education.
- [30] Maffulli, R., and He, L., 2014. "Wall temperature effects on heat transfer coefficient for high-pressure turbines". *Journal of Propulsion and Power*, **30**(4), pp. 1080–1090.
- [31] Maffulli, R., and He, L., 2017. "Impact of Wall Temperature on Heat Transfer Coefficient and Aerodynamics for Three-Dimensional Turbine Blade Passage". *Journal of Thermal Science and Engineering Applications*, **9**(4), 04. 041002.
- [32] Zhang, Q., and He, L., 2014. "Impact of Wall Temperature on Turbine Blade Tip Aerothermal Performance". *Journal of Engineering for Gas Turbines and Power*, **136**(5), 01. 052602.
- [33] Shadloo, M. S., and Hadjadj, A., 2017. "Laminar-turbulent transition in supersonic boundary layers with surface heat transfer: A numerical study". *Numerical Heat Transfer, Part A: Applications*, **72**(1), pp. 40–53.
- [34] Braslow, A. L., 1966. "A review of factors affecting boundary-layer transition". *NASA Technical Note D-3384*.
- [35] Buntin, D. A., Maslov, A. A., and Gromyko, Y. V., 2012. "The effect of temperature of a cone nose-tip on the spectra of disturbances in the hypersound boundary layer". *Technical Physics Letters*, **100**(241603).
- [36] Fedorov, A., Soudakov, V., Egorov, I., Sidorenko, A., Gromyko, Y., Bountin, D., Polivanov, P., and Maslov, A., 2015. "High-speed boundary-layer stability on a cone with localized wall heating or cooling". *AIAA Journal*, **53**(9), pp. 2512–2524.
- [37] Zhu, Y., Zhu, W., Gu, D., Lee, C., and Smith, C., 2021. "Hypersonic transition over a heated wall". *Physics of Fluids*, **33**(10), p. 101706.
- [38] Schäfer, P., Severin, J., and Herwig, H., 1995. "The effect of heat transfer on the stability of laminar boundary layers". *International Journal of Heat and Mass Transfer*, **38**(10), pp. 1855–1863.
- [39] Özgen, S., 2004. "Effect of heat transfer on stability and transition characteristics of boundary-layers". *International Journal of Heat and Mass Transfer*, **47**(22), pp. 4697–4712.
- [40] Liepmann, H. W., and Fila, G. H., 1947. "Investigations of effects of surface temperature and single roughness elements on boundary-layer transition". *NACA Technical Note No. 1196*.
- [41] Reshotko, E., and Tumin, A., 2004. "Role of transient growth in roughness-induced transition". *AIAA Journal*, **42**(4), pp. 766–770.
- [42] Arnal, D., and Vermeersch, O., 2011. "Compressibility effects on laminar-turbulent boundary layer transition". *International Journal of Engineering Systems Modelling and Simulation*, **3**(1-2), pp. 26–35.
- [43] Rubini, R., Maffulli, R., and Arts, T., 2018. "Effect of the gas to wall temperature ratio on the bypass transition". *ASME Paper No. GT2018-76214*.
- [44] Back, L. H., Cuffel, R. F., and Massier, P. F., 1969. "Laminar, Transition, and Turbulent Boundary-Layer Heat-Transfer Measurements With Wall Cooling in Turbulent Airflow Through a Tube". *Journal of Heat Transfer*, **91**(4), 11, pp. 477–487.
- [45] He, L., 2021. "Averaging for High Fidelity Modeling - toward Large Eddy Simulations in Multi-Passage Multi-Row Configurations". *Journal of Turbomachinery*, **143**(2), 02. 021002.